NUMERICAL MODELING OF TIDAL WAVE RUNUP

By Vasily V. Titov[1] and Costas Emmanuel Synolakis[2]

ABSTRACT: A numerical solution for the 2 + 1 (long-shore and onshore propagation directions and time) nonlinear shallow-water wave equations, without friction factors or artificial viscosity is presented. The models use a splitting method to generate two 1 + 1 propagation problems, one in the onshore and the other in long-shore direction. Both are solved in characteristic form using the method of characteristics. A shoreline algorithm is implemented, which is the generalization of the earlier 1 + 1 algorithm used in the code VTCS-2. The model is validated using large-scale laboratory data from solitary wave experiments attacking a conical island. The method is applied then to model the 1993 Okushiri, Japan, the 1994 Kuril Island, Russia, and the 1996 Chimbote, Peru tsunamis. It is found that the model can reproduce correctly overland flow and even extreme events such as the 30-m runup and the 20-m/s inundation velocities inferred during field surveys. The results suggest that bathymetric and topographic resolution of at least 150 m is necessary for adequate predictions, while at least 50 m resolution is needed to model extreme events, contrary to intuitive expectations that long waves would not interact with morphological features of such short scales.

INTRODUCTION

Tidal waves or tsunamis are long water waves generated by impulsive geophysical events such as submarine earthquakes, coseismic coastal or submarine landslides, and volcanos. Until recently, catastrophic tidal waves generally had been believed to occur—at worst—once every 10 years around the Pacific Rim.

In the 4-year period of 1992–1996, eight large earthquakes generated tsunamis with runup heights ranging from 5 to 30 m. Before these events, the last major tsunami of similar magnitude occurred in 1983. These events caused extensive inundation and claimed the lives of approximately 2,000 people. They were all investigated by an ad hoc group of primarily Japanese and American scientists referred to as the International Tsunami Survey Team (ITST). The ITST produced high-quality inundation data, at exactly the time when inundation codes had started addressing the computational barriers of the notoriously difficult shoreline calculation. The watershed event was the Nicaraguan tsunami of September 1, 1992. The initial numerical computations demonstrated the inability of the available codes to model, even to first order, the inundation patterns. These discrepancies fueled speculation whether it was the seismological models, which predicted incorrect initial conditions, or the hydrodynamic models, which did not simulate properly the propagation and runup. Subsequent events confirmed that discrepancies exist, but advances in the hydrodynamic codes have reduced them substantially. These advances and results that will be presented here suggest that given correct initial conditions, inundation computations primarily are limited by the availability of bathymetry and topography data of sufficient resolution.

The 1 + 1 runup problem (one propagation direction and time) for physically realistic initial conditions was only solved in the past 10 years, despite the existence of the analytical transformation of Carrier and Greenspan (1958), which allowed the calculation of the runup of a monochromatic wave on a plane beach. The transformation was used by Synolakis (1987) who showed how to link the linear and nonlinear theory results, calculated the runup of a solitary wave on a plane beach, and derived asymptotic results relating the runup with initial wave height and beach slope. The detailed history of the 1 + 1 problem is reviewed in Liu et al. (1991), Shuto (1991), and Titov and Synolakis (1995a). Hibberd and Peregrine (1979) and Iwasaki and Mano (1979) presented a shoreline algorithm to study the evolution of long waves, using the nonlinear shallow-water (NSW) wave equations. However, the latter shoreline algorithm was not robust (Synolakis 1989) and was based on ad hoc assumptions to stabilize the computations. Nonetheless, Hibberd and Peregrine's (1979) method did provide the basis for the development of very robust algorithms as shown in a series of papers by Kobayashi et al. (1987, 1992). Raubenheimer et al. (1996) even used Kobayashi's method for calculating the runup of wind waves. Zelt (1991) presented a finite-element solution to the Boussinesq equations. Titov and Synolakis (1995a) presented the first numerical solution of the 1 + 1 equations without adding artificial viscosity and/or friction factors. Tadepalli and Synolakis (1995, 1996) showed that the coastal manifestation of a tidal wave is "N-wave like" and proved that the runup of leading-depression (LDN) waves is higher than the runup of leading-elevation (LEN) waves. All of the foregoing formulations are based on the depth-averaged linear shallow-water (LSW) wave equations and the NSW. In a series of papers, Grilli et al. (1994), and Grilli and Subramanya (1996) solved the complete potential flow problem of limiting solitary waves climbing up a sloping beach and discussed the limitations of lower orders of approximation such as the NSW in predicting long-wave evolution and runup.

The 2 + 1 propagation problem (two propagation directions and time) has been considerably more elusive to solve. Although laboratory data and exact solutions were available for 1 + 1 problems, the first laboratory data on 2 + 1 propagation were presented only recently (Briggs et al. 1995). Brocchini and Peregrine (1996) presented a weakly 2 + 1 semianalytical solution of the NSW equations. Fujima (1995) and Kanoglu and Synolakis (1995) presented linear theory solutions for the runup of solitary waves on islands. The first breakthrough in numerical computation was Shuto's (1991) solution of the 2 + 1 NSW. The original method did not calculate runup. Instead, the computation was stopped at some reference depth to avoid both breaking and the shoreline computation. The maximum wave height at that depth was used to infer the runup, and such models are now referred to as threshold-type models. Shuto's original method was the basis for further evolved numerical methods, which have now been field-tested and perform realistic inundation computations (Liu et al. 1995; Takahashi et al. 1995). Titov and Synolakis (1995b) presented another 2 + 1 solution, which does not need the addition of ad hoc friction factors, while Masamura and Fujima (1995)

[1]Pacific Marine Environmental Lab., NOAA, Seattle, WA 98115.
[2]Dept. of Civ. Engrg., Univ. of Southern California, Los Angeles, CA.

Note. Discussion open until January 1, 1999. To extend the closing date one month, a written request must be filed with the ASCE Manager of Journals. The manuscript for this paper was submitted for review and possible publication on November 25, 1997. This paper is part of the ***Journal of Waterway, Port, Coastal, and Ocean Engineering***, Vol. 124, No. 4, July/August, 1998. ©ASCE, ISSN 0733-950X/98/0004-0157–0171/$8.00 + $.50 per page. Paper No. 17205.

J. Waterway, Port, Coastal, Ocean Eng. 1998.124:157-171.

presented a model based on the Euler equations. Models that perform 2 + 1 runup computations are not referred to as inundation models. None of these models can or should calculate the postbreaking evolution of breaking waves. Yet, all 2 + 1 existing solutions of NSW equations have proven to be robust enough to calculate the wave evolution of mildly breaking waves, through breaking to the maximum penetration point, without reproducing any of the details of the breaking waves. This fortuitous capability of the NSW equations is very useful in modeling because a given field manifestation of a tidal wave may break on very gentle beaches of the target coastline, while it may evolve unbroken on steeper slopes, often adjacent to the former ones.

Despite these advances, the unresolved question of identifying whether the inadequate resolution of the initial conditions or the difficulty of the shoreline computation are responsible for discrepancies between field runup measurements and model predictions persists. However, an argument could be made that, given correct initial conditions, well-posed hydrodynamic computations are limited only by the resolution of bathymetric and on-land topographic data. In contrast, the seismological data used to define the initial condition for the evolution calculations are quite sensitive to the proximity of the tsunamigenic faulting to strong-motion stations and to the availability of historic records for that fault area. Until recently, seismologists were not interested in the first-order details of the seafloor-interface motions because seismological models only provide the average seafloor displacement over the entire deformed area. Hydrodynamic modelers routinely use elastic models with the seismic parameters as input to calculate details of the deformation, which then translate to the initial condition of the evolution problem. Imamura et al. (1993) pioneered the practice of varying the seismic parameters as provided by the fault solutions to improve the runup predictions and showed that this variation converged to parameters geophysically realistic within the margin of error of seismological computations. However, still unresolved is the level of bathymetric and topographic resolution needed for accurate predictions, the quantitative comparison of threshold-type models with inundation models and field data, and the relative effects of the friction factor.

Here, a new method of solution of the 2 + 1 NSW equations will be presented. The method will be described and validated against the large-scale experiments of Briggs et al. (1995). It will be used then to model three actual events: the 1994 Kuril Islands, the 1996 Chimbote, Peru, and the 1993 Okushiri, Japan tsunamis. Three different approximations to runup computations are used, depending on the resolution of the available bathymetric and topographic data. This study does not address the question of the resolution of the initial conditions from fault solutions. Important as it is, it is largely a problem for interface seismology. However, a brief description of the determination of the initial condition is provided.

The purpose of the study is to show that given well-defined initial data, the hydrodynamic problem is now solvable. It is essential to identify the differences between bathymetric and topographic resolution versus numerical grid resolution and it will be shown that the latter is less important than the former. The presented results also suggest that the tidal wave velocities during runup are unexpectedly large. Also, for certain topographies, the extreme over the affected area velocities do not occur at the same locales as the extreme runup. In those cases, the inundation area may correlated more strongly with the extreme velocity contours than with the runup contours.

NUMERICAL MODEL

Mathematical Formulation

The depth-averaged 2 + 1 shallow-water wave equations (NSW) are used to model this phenomenon. Despite certain limitations (Liu et al. 1991), these equations have proven capable to model many important physical characteristics of tsunami propagation, including wave breaking and bore runup on mild and steep beaches. Recent studies (Titov and Synolakis 1995) have shown that this approximation works reasonably well even in the case of relatively short (length-to-depth ratio less than 10) mildly breaking waves. Although the equations cannot resolve the dynamics of the breaking front, they adequately model the overall wave behavior and give accurate estimates of the runup over a wide range of wave and beach-slope parameters.

The 2 + 1 NSW equations are

$$h_t + (uh)_x + (vh)_y = 0 \tag{1a}$$

$$u_t = uu_x + vu_y + gh_x = gd_x \tag{1b}$$

$$v_t + uv_x + vv_y + gh_y = gd_y \tag{1c}$$

where $h = \eta(x, y, t) + d(x, y, t)$; $\eta(x, y, t)$ = wave amplitude; $d(x, y, t)$ = undisturbed water depth; $u(x, y, t)$ and $v(x, y, t)$ = depth-averaged velocities in the onshore x and long-shore y directions, respectively; and g = acceleration of gravity.

The model does not include any bottom friction terms. Although the bottom friction does affect the dynamics of the runup process in the surf zone, there are several reasons for not using friction terms. The commonly used bottom friction model for evolution and inundation calculations is the Chésy formula with different types of roughness coefficient (Packwood and Peregrine 1981; Kobayashi et al. 1987; Kowalik and Bang 1987; Liu et al. 1995). This formula is an empirical relationship developed from steady channel flows, so it may not reflect the dynamics of the rapid runup process adequately. Also, there is no consensus on a proper form of the roughness coefficient in the formula. A number of studies have been devoted to designing a proper roughness coefficient instead of the commonly used Manning's coefficient (Fujima and Shuto 1989; Synolakis and Skjelbreia 1993). On the other hand, several studies have shown that an unsteady flow during runup is not very sensitive to changes in the roughness coefficient value (Packwood and Peregrine 1981; Kobayashi et al. 1987; Zelt 1991). Any moving boundary computation induces numerical friction near the tip of the climbing wave (except in a Lagrangian formulation), complicating the proper choice of the friction coefficient and separating the effects of the friction terms from numerical dissipation. Summarizing, the choice of roughness coefficient in numerical models at the present state of science appears arbitrary and usually is chosen to make results fit a given laboratory experiment or field event but is otherwise difficult to determine a priori. Because the goal is the evaluation of extreme runup and inundation velocities, which friction can only reduce in some cases, it is expected that the results will be conservative compared with results from models that incorporate friction.

A variety of boundary and initial conditions can be specified for the NSW equations. To solve the problem of tsunami generation caused by bottom displacement, the following initial conditions are specified:

$$d(x, y, t) = d_0(x, y, t); \quad t \le t_0 \tag{2a}$$

$$d(x, y, t) = d_0(x, y, t_0); \quad t > t_0 \tag{2b}$$

where $d_0(x, y, t)$ = a function describing the bottom movement during the time period $0 \le t \le t_0$. Usually, t_0 is assumed to be small, so that the bottom movement is considered as an instantaneous vertical displacement. This assumption may not be entirely appropriate for very slow events occurring very close to the shoreline, but it is the standard practice in all evolution and inundation models and probably will continue to be until demonstrated inadequate. The determination of the

J. Waterway, Port, Coastal, Ocean Eng. 1998.124:157-171.

static bottom deformation $d_0(x, y)$ is accomplished using what are referred to as displacement models and is discussed briefly later.

To produce the wave entering into the computational area through the boundary $y = y_b$, the following conditions are specified on the boundary:

$$v(x, y_b, t) = v_0(x, y_b, t); \quad h(x, y_b, t) = h_0(x, y_b, t) \quad (3a,b)$$

where $v_0(x, y, t)$ and $h_0(x, y, t)$ = functions describing velocity and amplitude variations of the incoming wave on the boundary. The proper boundary conditions should be specified for open-sea and land boundaries. These conditions will be discussed later in this chapter.

Splitting Technique

For arbitrary topography and bottom displacements, the system of (1) has to be solved numerically. Consider the finite differences (FDs) algorithm based on the splitting method, also known as the method of fractional steps (Yanenko 1971). This method reduces the numerical solution of the 2 + 1 problem into consecutive solutions of two "instantaneous" 1 + 1 problems. This is achieved by splitting the governing system of (1) into a pair of systems, each containing only one space variable as follows:

$$\left\{\begin{array}{c} h_t + (uh)_x = 0 \\ u_t + uu_x + gh_x = gd_x \\ v_t + uv_x = 0 \end{array}\right\} \quad \text{and} \quad \left\{\begin{array}{c} h_t + (vh)_y = 0 \\ v_t + vv_y + gh_y = gd_y \\ u_t + vu_y = 0 \end{array}\right\} \quad (4a,b)$$

Although, the conventional procedure for the splitting method is the use of implicit schemes, the two systems of (4) are solved sequentially at each time step using an explicit FD scheme. The implicit approach works effectively for elliptic and parabolic equations. Splitting gives a substantial reduction in the number of operations compared with application of the implicit scheme directly to two-dimensional elliptic or parabolic equations (Fletcher 1991, Ch. 8.5). The system in (1) is a hyperbolic quasi-linear system and explicit methods have proven to be very efficient. It was found advantageous to use the splitting method in combination with an explicit FD technique. The main advantage is the ability to solve directly the characteristic form of the 1 + 1 equations. The characteristic analysis helps to establish a well-posed boundary value problem (BVP) for the numerical method and also allows for an efficient FD realization (Titov and Synolakis 1995a).

Each of the systems of (4) is a hyperbolic quasi-linear system with all real and distinct eigenvalues. It can be written in characteristic form as follows:

$$p_t + \lambda_1 p_x = gd_x; \quad q_t + \lambda_2 q_x = gd_x; \quad v' + \lambda_3 v' = 0 \quad (5a-c)$$

Here, the Riemann invariants of this system are

$$p = u + 2\sqrt{gh}; \quad q = u - 2\sqrt{gh}; \quad v' = v \quad (6a-c)$$

and the three distinct eigenvalues are

$$\lambda_1 = u + \sqrt{gh}; \quad \lambda_2 = u - \sqrt{gh}; \quad \lambda_3 = u \quad (7a-c)$$

Eqs. (5*a*) and (5*b*) constitute a 1 + 1 NSW problem. At every time step, a long-wave propagation problem will be solved along the current coordinate, defined by the 1 + 1 NSW equations and one more equation describing a momentum flux in the direction normal to the current coordinate. The method developed for 1 + 1 long-wave propagation and runup (Titov and Synolakis 1995a) will be applied to the solution of the system in (5).

To describe the overall procedure in FD terms, let u^n, v'^n, h^n for time instant $t = n\Delta t$ be known. The algorithm computes u^{n+1}, v'^{n+1}, h^{n+1} at the next time step $t = (n + 1)\Delta t$ through the following steps.

The primitive variables u^n, v^n, h^n are converted into the Riemann invariants p^n, q^n, v'^n using transformation in (6).

The $p^{n+1/2}$, $q^{n+1/2}$, $v'^{n+1/2}$ are computed by solving (5) numerically along the x-coordinate.

The $p^{n+1/2}$, $q^{n+1/2}$, $v'^{n+1/2}$ are converted back to the primitive variables $u^{n+1/2}$, $v^{n+1/2}$, $h^{n+1/2}$ using the inverse transformation.

The above three steps are repeated for the y-coordinate to compute the values u^{n+1}, v'^{n+1}, h^{n+1}. Note, that the Riemann invariants are different during this step, because u and v interchange with each other in (6) and (7).

Boundary Conditions for Fixed Boundaries

The splitting method requires the consecutive solutions of 1 + 1 systems every time step. Therefore, boundary conditions must be established for the 1 + 1 problem and the method of characteristics is applied to formulate well-posed BVPs.

The system of (5) is a hyperbolic quasi-linear system with all real and distinct eigenvalues in (7). It has three families of characteristic lines with slopes λ_1, λ_2, and λ_3: λ_1 is always positive, λ_2 is negative everywhere the Froude number is less than one, and λ_3 can be either positive or negative. A well-posed BVP requires the number of boundary conditions for Riemann invariants be equal to the number of outgoing characteristic lines for this boundary. Therefore, one or two boundary conditions are necessary on each boundary, depending on the sign of λ_3 on the specific boundary.

The boundary conditions for a totally reflective left boundary are

$$p = -q; \quad v' = 0 \quad (8a,b)$$

whereas the reflective conditions for the right boundary are

$$q = -p; \quad v' = 0 \quad (9a,b)$$

Gustafsson and Kreiss (1979) used this approach to develop absorbing boundary conditions for time-dependent problems. A totally absorbing boundary allows waves to go through (absorb), but it does not allow any waves to reflect back into the computation region. In characteristic terms, the invariants of outgoing characteristics do not bring anything back into the computational area. For the right boundary, the requirement of no wave motion on the characteristics implies that $u = 0$, $v = 0$, $\eta = 0$, $q = -2\sqrt{gd}$, and $v' = 0$. In addition, it is assumed that the water depth is constant outside the area of computation and equal to the depth at the right boundary d_n. Then (5) implies that q is constant on that boundary. Therefore, the appropriate conditions are

$$q = -2\sqrt{gd_n}; \quad v' = 0 \quad (10a,b)$$

For the left boundary, the absorbing conditions are

$$p = 2\sqrt{gd_n}; \quad v' = 0 \quad (11a,b)$$

The runup computations require a moving boundary condition for the tip of the shoaling wave. Titov and Synolakis (1995a) developed the moving boundary condition for 1 + 1 NSW equations. The same basic approach can be used for the runup boundary condition for the system in (5). It will be discussed briefly in the next section.

FD Scheme

The following explicit FD scheme is used for each equation of system in (5):

$$\frac{\Delta_t p_i^n}{\Delta t} + \frac{1}{\Delta x_{i-1} + \Delta x_i}\left[\lambda_i^n(\Delta_{-x} + \Delta_x)p_i^n - 2\Delta t\lambda_i^n\Delta_x\left(\frac{\Delta_x}{\Delta x_i}\right)\lambda_i^n p_i^n\right]$$

$$= \frac{g}{\Delta x_{i-1} + \Delta x_i}\left[(\Delta_{-x} + \Delta_x)d_i^n - 2\Delta t\lambda_i^n\Delta_x\left(\frac{\Delta_x}{\Delta x_i}\right)d_i^n\right]$$

J. Waterway, Port, Coastal, Ocean Eng. 1998.124:157-171.

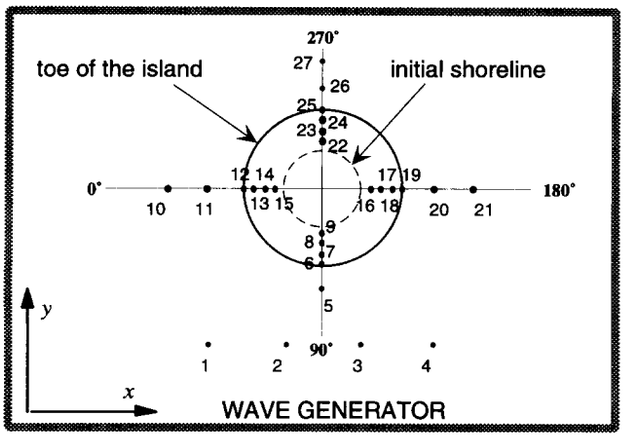

FIG. 1. Sketch of Basin and Location of Wave Gauges

(12)

where Δt = time increment; $\Delta x_i = x_{i+1} - x_{i-1}$ = space increment; p = one of the Riemann invariants; λ = corresponding eigenvalue; d = depth; and g = acceleration of gravity. The following operator notations are used:

$$f_i^n = f(x_i, t_n)$$

$$\Delta_t f_i^n = f(x_i, t_n + \Delta t) - f(x_i, t_n)$$

$$\Delta_x f_i^n = f(x_i + \Delta x_i, t_n) - f(x_i, t_n)$$

$$\Delta_{-x} f_i^n = f(x_i, t_n) - f(x_i - \Delta x, t_n)$$

This scheme allows for the spatial grid with a variable space step Δx_i. The condition for stability is the Courant-Friedrichs-Levy criterion

$$\Delta t \leq \min_i \frac{\Delta x_i}{|u_i| + \sqrt{g h_i}} \tag{13}$$

The FD scheme in (12) is used for the computation of the unknown variables p, q, and v' in the interior grid points of the computational area. However, these equations cannot be used to compute boundary values. At those points, the boundary conditions in (8)–(11) determine only two of the three invariants. The other value on the boundary (the value of the Riemann invariant on the incoming characteristic) is computed using one of the governing equations in (5) by the upwind FD scheme

$$p_b^{n+1} = p_b^n - \frac{\Delta t}{\Delta x_b} [\lambda_i^n (\Delta_{-x} p_b^n) - g(\Delta_{-x} d_b^n)] \tag{14}$$

where p_b, d_b = values of the variables on the boundary.

During shoaling the wavelength of tidal waves becomes shorter. Therefore, calculations using a uniform grid throughout the computational domain may suffer either loss of accuracy in the nearshore from too coarse grid or loss of efficiency through the use of a very fine grid. Either approach does not produce consistent resolution. In the present method, a variable grid is used in each direction. The variable grid can create a consistent resolution for a one-dimensional domain (Titov and Synolakis 1995a), or a cylindrical two-dimensional domain, because the depth is changing predominantly only along one direction (Titov 1989).

To model tsunami wave propagation in areas with complex bottom profiles containing complicated shoreline patterns and islands, an additional nested grid is needed for the nearshore computations. The nested grid has finer grid spacing for efficient computation of the shorter long waves in the nearshore area. A special algorithm has been developed to create automatically nested grids where the depth is less than a certain threshold value. The same FD numerical scheme in (12) computes the wave field on both grids at the same time. The computed values are interpolated on the boundaries between the grids every time step to provide a continuous flow of information between the different grid formulations. This approach allows for computations in large complicated areas with a minimum loss of accuracy due to inconsistent resolution of the FD grid.

Moving Boundary Condition

To calculate the evolution on the dry bed, it is necessary to use moving boundary conditions. The Froude number may be greater than one near the shoreline point, implying that all characteristic families have the same inclination in this region. Hence, it is impossible to use the direct relationships between the Riemann invariants of the type in (8)–(11) near the shoreline. Therefore, approximations of the boundary values from previous space nodes are used.

The shoreline algorithm uses a time-dependent space step $\Delta x(t)$ corresponding to the last node of the computational area. The objective is to maintain the shoreline boundary point on the surface of the beach during the computation. Therefore, the length of the last space step $\Delta x(t)$ is adjusted every time step, so that the shoreline point is at the intersection of the beach with the horizontal projection of the last "wet" point. The value of the velocity on the shoreline node is equal to the velocity on the previous wet point. The 1 + 1 procedure is described in great detail in Titov and Synolakis (1995a). Because the algorithm is solving pairs of consecutive 1 + 1 problems, the same method will be used here.

VERIFICATION OF MODEL

The 1 + 1 computations described in Titov and Synolakis (1995a) validated different aspects of numerical performance of the FD scheme in (12) and showed it capable of calculating the runup of mildly breaking, plunging waves on a plane beach. Because exactly the same scheme is used for the 2 + 1 model through splitting, the dispersion and mass conservation properties are the same as reported for the 1 + 1 scheme. To test the overall 2 + 1 algorithm, a numerical simulation of the conical island experiments of Briggs et al. (1995) was performed.

A large-scale laboratory experiment of tsunami runup on a circular island was conducted recently at the U.S. Army Engineer Waterways Experiment Station by Briggs et al. (1995), also discussed in Liu et al. (1995). They used a large 30-m-wide and 25-m-long basin with a conical island near its center to study the runup of solitary waves. A directional spectral wave generator with 60 individual paddles produced plane solitary waves with specified crest lengths and wave heights propagating toward the island. Twenty-seven wave gauges were distributed around the basin as shown in Fig. 1, to record the free-surface displacement. The highest excursion of the shoreline was measured around the island after each run at 20 locations. The laboratory data from these experiments provide an excellent validation test for 2 + 1 long-wave models; in fact they were used as a benchmark problem for the International Workshop on Long Wave Runup, Friday Harbor, Washington for comparisons with the predictions of numerical models (Yeh et al. 1996).

The basin was discretized with a mesh size $\Delta x = \Delta y = 0.15$ m over the flat bottom and with $\Delta x = \Delta y = 0.09$ m over the sloping beach of the conical island. The $\Delta t = 0.02$ s was used. The boundary $y = 0$ of the computational domain is the wave generator. The movement of the generator paddles was modeled by inputing the values of the velocity of the paddle at

J. Waterway, Port, Coastal, Ocean Eng. 1998.124:157-171.

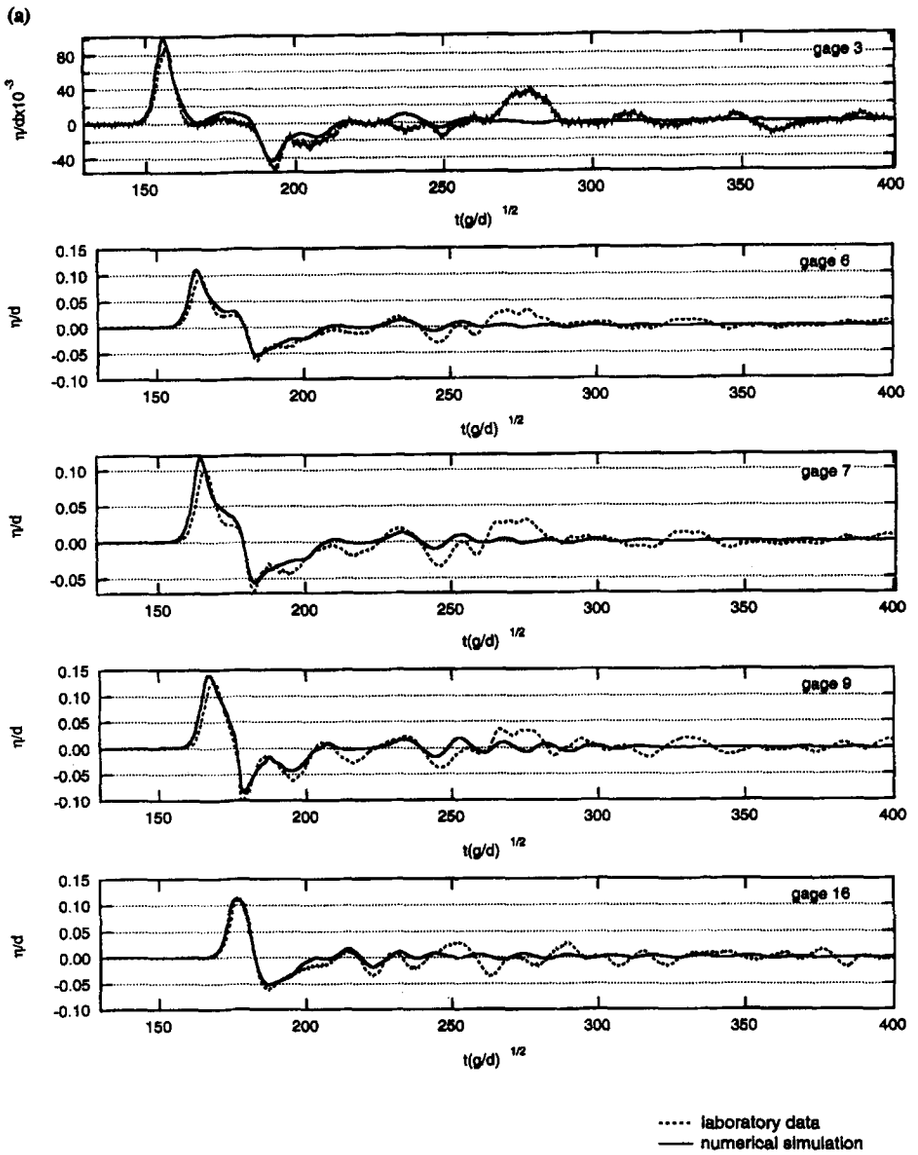

FIG. 2. Comparison among Computed (Solid Lines) and Laboratory Records (Dots) for $H = 0.1$ Wave, Gauges 3, 6, 7, 9, 18, 16, 22, 24, 25, and 26

each time step. The corresponding boundary condition for the system in (5) is

$$p_0^n = u_0^n + 2\sqrt{gd_0} \tag{15}$$

where $p_0^n = p(0, t + n\Delta t)$ = boundary value of the Riemann invariant; $u_0^n = u(0, t + n\Delta t)$ = velocity of the paddle movement computed from the paddle trajectory used in the experiment; and d_0 = depth of the constant depth region. On the computational boundary behind the island defined by $0 < x < 30$ m and $y = 25$ m, an absorbing boundary condition was specified. Moving boundary inundation computations were performed around the conical island shoreline.

Two cases were modeled where the whole length of the wave generator was used. The dimensionless amplitudes $H = \eta/d$ of the modeled waves were $H = 0.1$ and $H = 0.2$, corresponding to the highest two among the laboratory waves of Briggs et al. (1995). These are rather severe tests of the algorithm, because the waves are steeper than most geophysical tsunamis.

Fig. 2 shows the comparison among the computed time series and the wave gauge records of the experiment for the $H = 0.1$ wave. The comparison shows that the computed wave simulates the incident wave and the first reflection off the conical island very well. The tail of the laboratory record differs from the computed profiles because the boundary absorption characteristics are different between the numerical and the laboratory models. In the laboratory manifestation, horsehair-type absorbers were used and, although small, reflection from the boundaries was observed during the experiments. Because the reflection coefficient was not measured for this absorber, the radiating or totally absorbing boundary conditions [see (10) and (11)] were used for the computations. These conditions assume no boundaries around the modeled area. Therefore, there is no reflection off the computational boundaries, but it is evident on the experimental records.

The experimental manifestation of the $H = 0.1$ wave breaks only in one location, on the back of the island where the trapped waves propagating from opposite sides collide with each other. The computed profile on gauge 22 suggests that wave breaking did not seriously affect the model prediction. In NSW, breaking manifests itself as a discontinuity of the solution of the nonlinear equations in (1). It has been argued by Meyer (1986) that this discontinuity does not really represent physical breaking, but only the breakdown of the as-

J. Waterway, Port, Coastal, Ocean Eng. 1998.124:157-171.

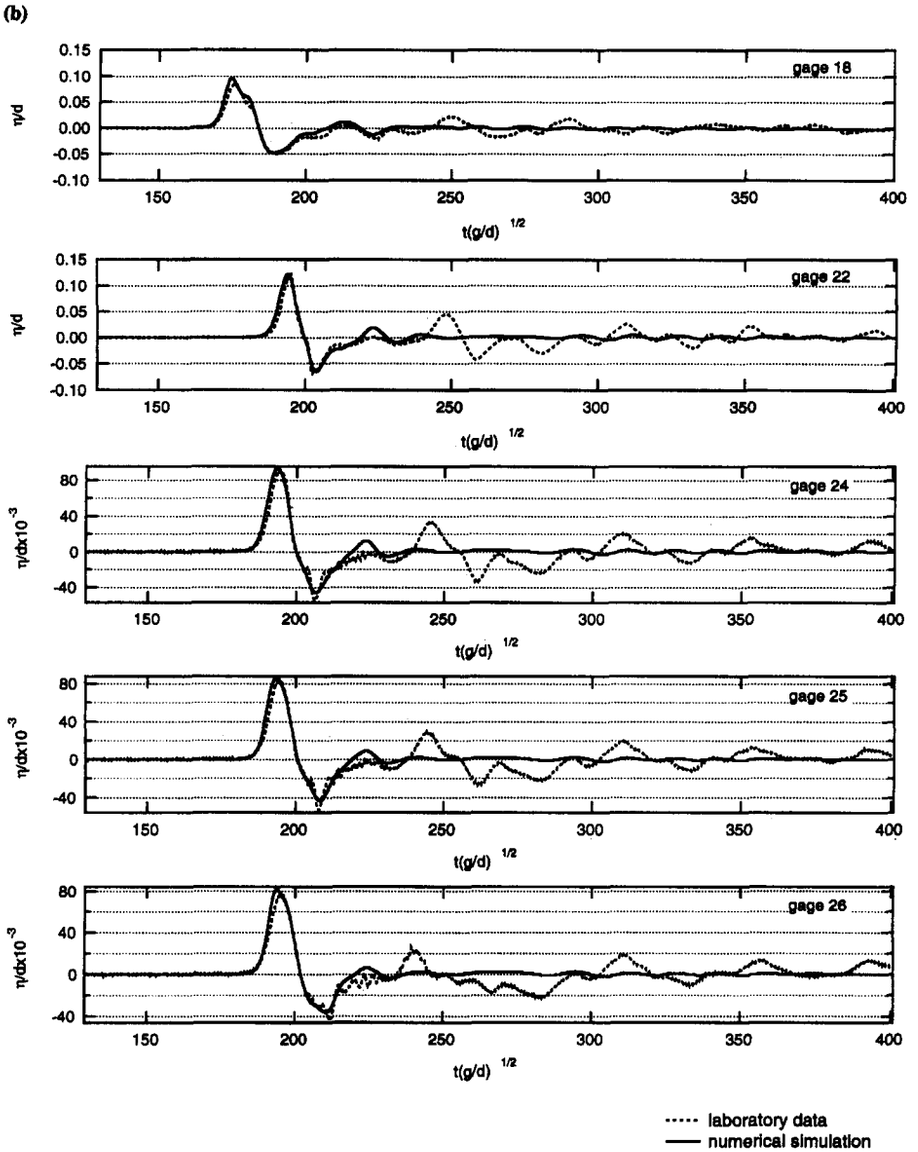

FIG. 2. (*Continued*)

sumptions of SW theory. Nonetheless, in all SW models, the onset of this discontinuity is identified as the onset of breaking. Imposing mass and momentum conservation at this discontinuity point allows the calculation of the evolution of the subsequent bore. In the computed solution, no bore conditions are specified. However, because mass and momentum are conserved, and because the numerical differencing is inherently dissipative, the computed solution reflects the overall evolution, without reproducing the details of the breaking front. Note that this also is observed in the analytical solutions of Synolakis (1987), in the numerical solutions of Kobayaski et al. (1987), Kobayashi and Wurjanto (1992), and Titov and Synolakis (1995).

Fig. 3 shows the comparison of the computed profiles with the laboratory measurements for the $H = 0.2$ wave at the same locations as in Fig. 1. This wave broke everywhere around the island as it evolved up the conical surface. The comparison suggests that the computed wavefront steepens faster than the laboratory manifestation, a well-known effect of NSW theory. The numerical model did not quite reproduce the height of splash off the lee side of the island where the two breaking waves crash into each other (gauge 24). Modeling of this effect would require a higher-order wave theory, which accounts for vertical accelerations.

Fig. 4 shows comparisons between the computed and measured runup values around the island for the $H = 0.1$ and $H = 0.2$ waves. Despite the extensive wave breaking of the $H = 0.2$ wave, the computed runup is in good agreement with the laboratory data, suggesting that only the horizontal velocities —at least in this parameter range—affect the runup to first order.

APPLICATION TO GEOPHYSICAL TSUNAMIS

When modeling a specific geophysical tsunami generated by a submarine earthquake, an appropriate initial condition has to be specified. This initial condition depends on the seafloor displacement, which is determined using what is referred to as displacement models.

The discussion of displacement models is beyond the scope of this paper. The specific model used here is a derivative of an elastic model first proposed by Gusiakov (1972), and fully described in Titov (1987). The basic assumption of the model is that the specific submarine earthquake under study triggers an instantaneous seafloor displacement on a level seafloor. Although this assumption is intuitively appropriate for events triggered at large water depths where the seafloor features are much smaller than the undisturbed water depth and for events

J. Waterway, Port, Coastal, Ocean Eng. 1998.124:157-171.

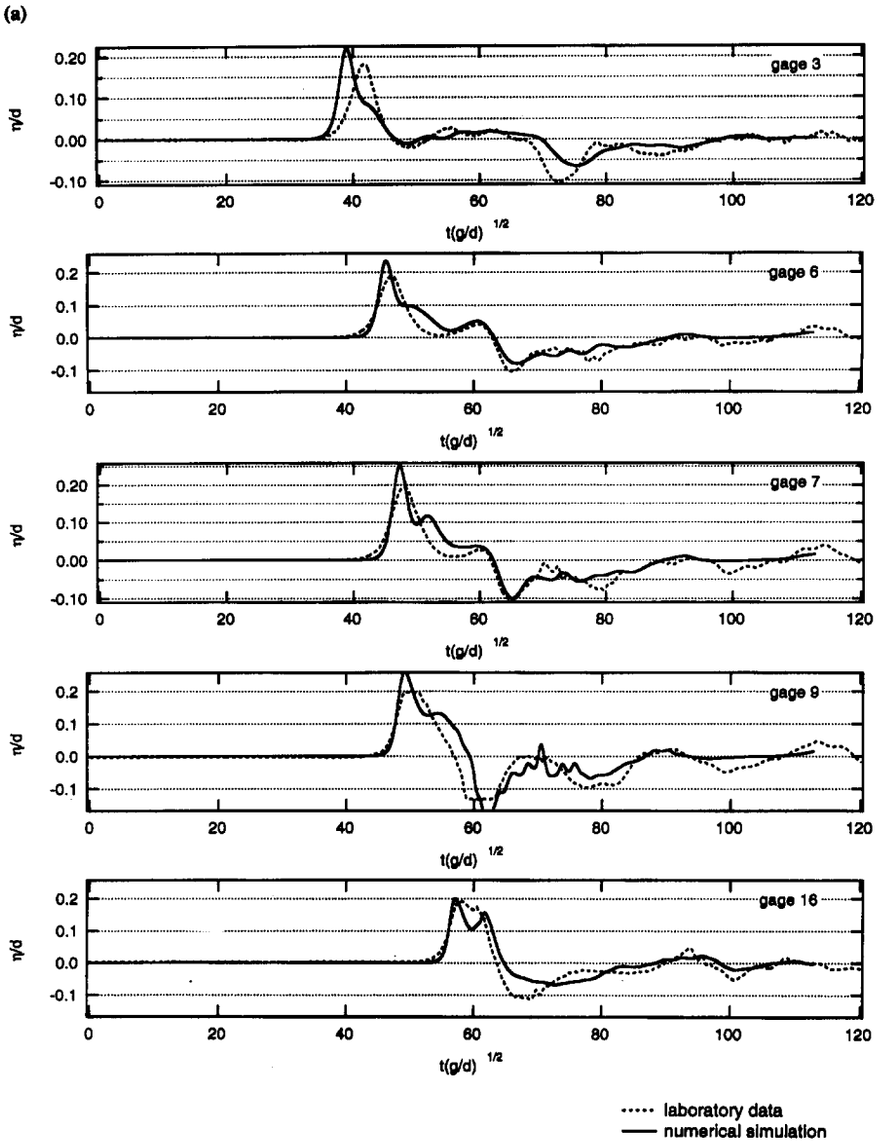

FIG. 3. Comparison among Computed (Solid Lines) and Laboratory Records (Dots) for $H = 0.2$ Wave, Gauges 3, 6, 7, 9, 18, 16, 22, 24, 25, and 26

far from their target coastlines, this assumption may not be entirely appropriate for nearshore submarine earthquakes in extremely shallow water. Nonetheless, since the work of Mansinha and Smylie (1971), this approach is the standard method for determining ground deformation, basically for lack of a better approach.

Briefly, an analysis of the seismic waves produces what is referred to as the Harvard central moment tensory (CMT) solution. The CMT solution specifies the length of the rupture plane L, the width W, the epicentral depth of the source h', the dip angle δ, the strike angle θ, and the average slip u_0. The moment magnitude M_0 is defined by

$$M_0 = \mu_e u_0 LW \tag{16}$$

where μ_e = rigidity of the earth's crust. Gusiakov's (1972) elastic model, as implemented by Titov (1997), then calculates the initial seafloor displacement $d_0(x, y)$ of (2).

Another difficulty with modeling geophysical tsunamis arises from the resolution of the available bathymetric and topographic data. (In the following discussion, the seafloor structure seaward of the coastline will be referred to as bathymetry and the inland structure as topography.) Although the calculation of tidal wave evolution over idealized bathymetries (such as that of a conical island) is only limited by the availability of computer memory, the calculation of actual events also is limited by the resolution of the bathymetric and topographic data over the propagation region of interest. In most areas, the only data available are from the TOPO-5 data set, (i.e., the undisturbed depth is defined over a 5-min or approximately 10-km grid) and there are no topographic data. In some cases, both bathymetric and topographic data exist down to a resolution of 20 m. In a few cases, the field survey teams documenting the inundation of a specific event also measured topographic transects at specific locations of interest, providing local high-resolution data.

Clearly, when no topographic data are available, any inundation (onshore) calculations are meaningless. Therefore, the following three different implementations of the described model have been developed, referred to as VTCS-3: (1) One where no inundation computations are performed but instead the 2 + 1 calculations stop at some threshold level offshore; (2) another where 2 + 1 computations are carried out to a threshold to provide an initial condition for a 1 + 1 computation where high-resolution transect data exist; and (3) a third 2 + 1 implementation, which carries the inundation computation inland to the point of maximum penetration. All three

J. Waterway, Port, Coastal, Ocean Eng. 1998.124:157-171.

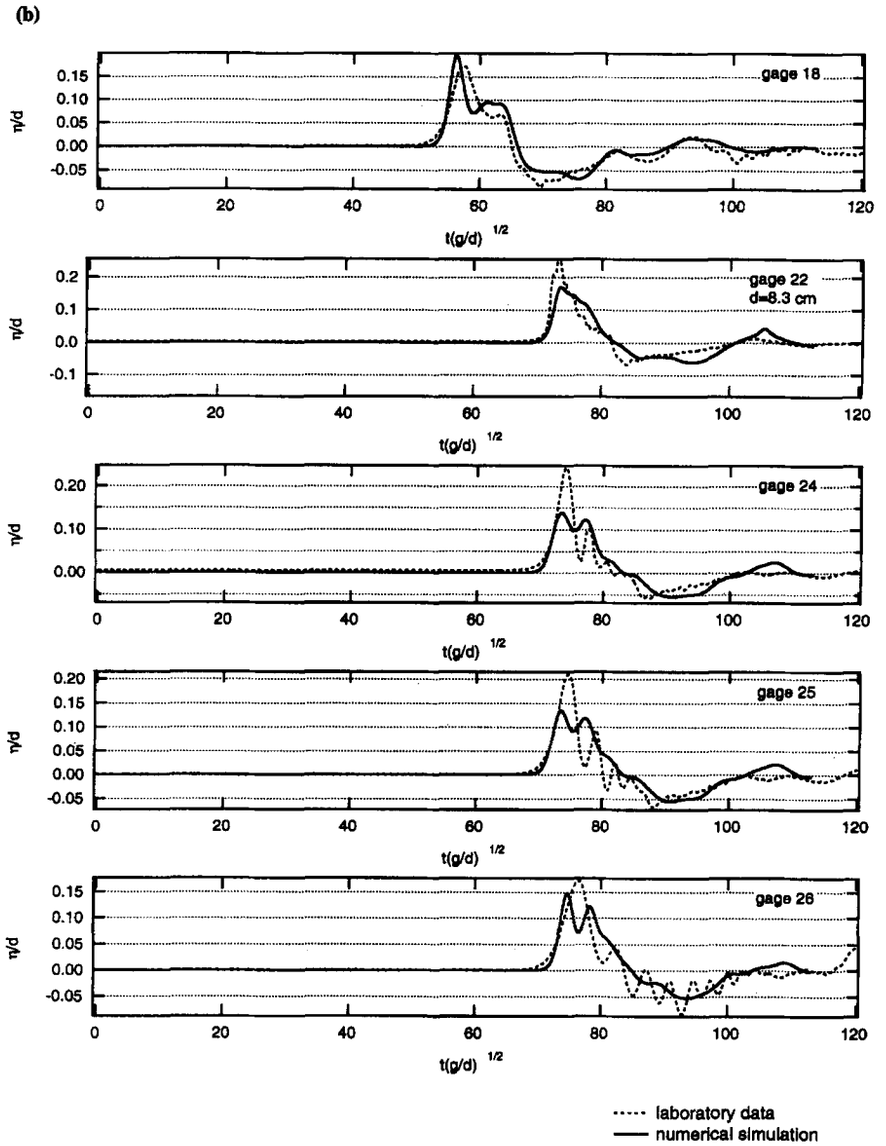

FIG. 3. (*Continued*)

implementations and differences between them will be discussed with specific examples from the 1994 Kurils Islands, the 1996 Peru, and the 1993 Okushiri tsunamis, respectively.

The 2 + 1 Threshold Computation Applied to 1994 Kurils Islands Tsunami

On October 4, 1994, at 13:23 GMT, an earthquake of magnitude M_w = 8.2 struck the southern region of Kuril Islands (Fig. 5). On Shikotan Island, located closest to the earthquake epicenter, the ground shaking was extremely intense and reported between 9/12 and 10/12 on the abridged Modified Mercalli Intensity Scale. A 1.8-m tsunami runup was reported immediately in Nemuro, Japan, and Pacific-wide tsunami warnings were issued, including all the coastal regions of Hawaii and the west coasts of the United States and Canada. Despite the large size of the wave, there were no casualties in the nearby islands, because the coastlines closest to the epicenter largely were uninhabited. Also, the South Kuril islands have experienced many large earthquake and tsunamis in the past, and the locals were prepared well for such natural disasters.

A tsunami reconnaissance survey was conducted from October 16 to 30, 1994, by the ITST, and the results are reported in Yeh et al. (1995). On Shikotan Island, measurements were made at 85 different locations around the island. They were fairly uniform with an average runup height of 6.07 m, suggesting that the tsunami wave was long enough not to have been affected by the local features of the coastline. The measured long penetration distances of the tsunami in spite of the dense vegetation also support the hypothesis of a fairly large wavelength of the climbing tsunami. Long waves with large periods would have sufficient time to flood all areas regardless of the local topography or resistance of dense vegetation. An eyewitness report in Malokurilskaya Bay indicated that the leading wave was an LEN (Tadepalli and Synolakis 1995, 1996), followed by an approximately 2.5-m depression wave. The resulting current was so swift that no ship could cross the bay entrance or approach the shore for the first 2 1/2 h, while a current speed of approximately 6 m/s was reported by an eyewitness. A subsequent bottom sounding showed that the water depth at the center of the bay changed from 5 to 8 m due to tsunami scouring effects.

Threshold-type 2 + 1 computations using VTCS-3 propagated the wave up to the 5-m contour. No inundation computations were performed. There was no high-resolution bathymetric data or topographical information available at the time of the modeling. Also, the wavelength of the Kuril tsu-

J. Waterway, Port, Coastal, Ocean Eng. 1998.124:157-171.

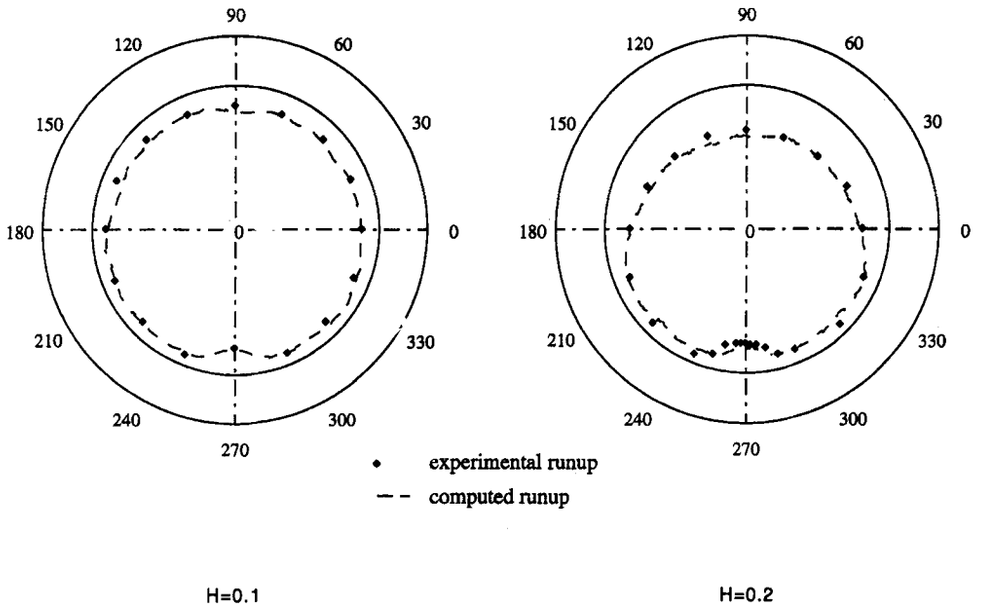

FIG. 4. Comparison between Computed and Observed Penetration on Conical Island for $H = 0.1$ and $H = 0.2$ Waves [Diagram Shows a Top View of Conical Island with Initial Shoreline (Solid Line), Measured Points of Maximum Runup (Diamonds), and Contours of Maximum Computed Wave Penetration (Dashed Line)]

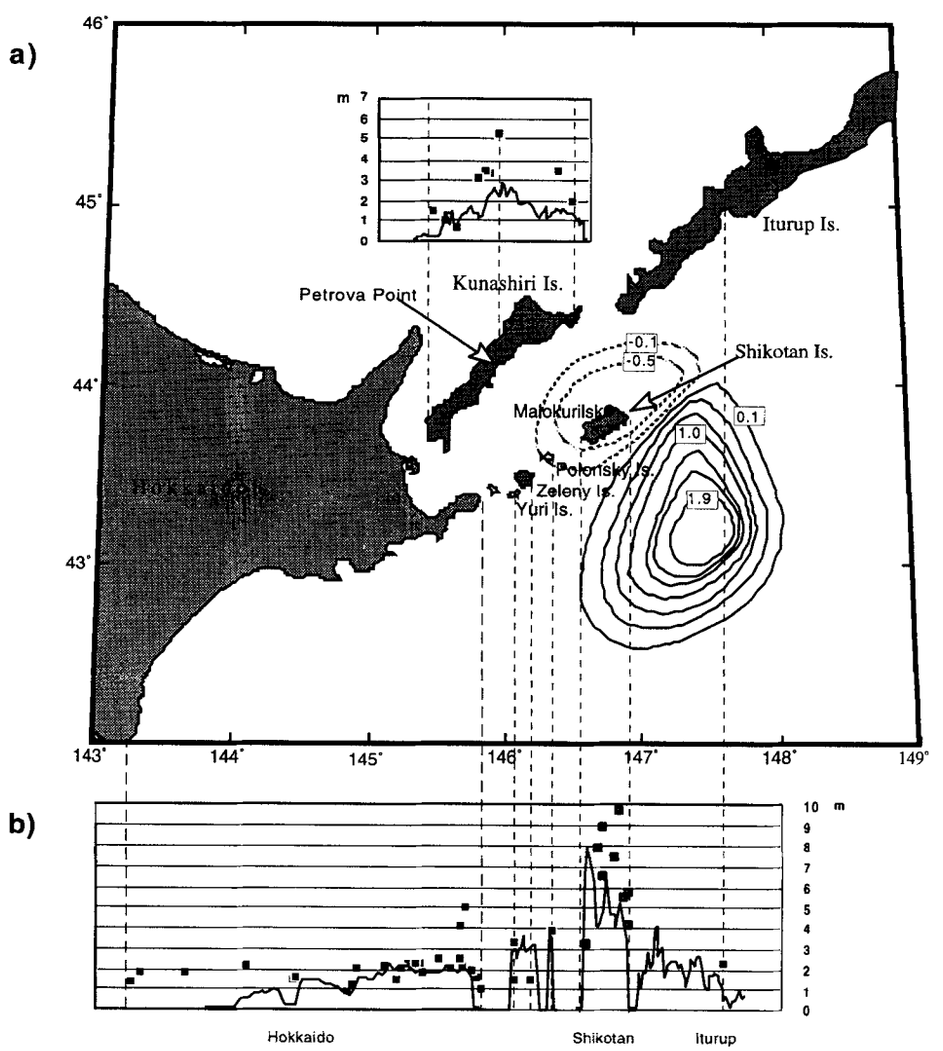

FIG. 5. Results of Computer Simulation of the 1994 Kuril Islands Tsunami: (a) Contours of Initial Seafloor Displacement Used as Initial Conditions; (b) Computed Wave Heights (Solid Lines) are Compared with Highest Runup Measurements (Dots) at Each Location

J. Waterway, Port, Coastal, Ocean Eng. 1998.124:157-171.

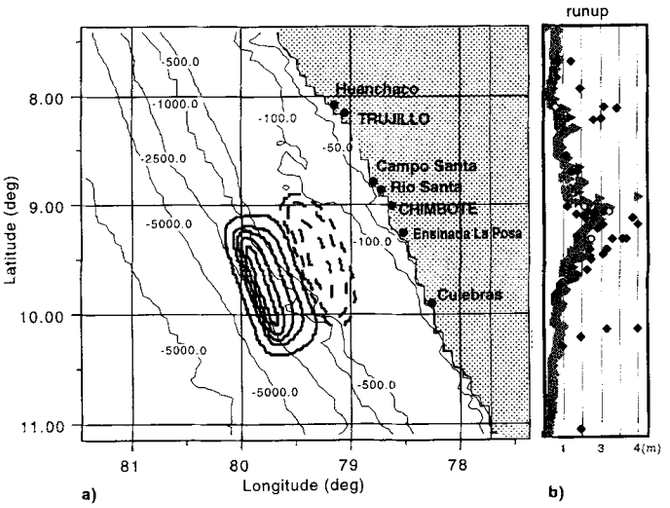

FIG. 6. (a) Contours of Seafloor Displacement for Peru Tsunami Used for Initializing VTCS-3 Computations; (b) Comparison between Measured Runup Heights (Black Diamonds), Computed with a Threshold 2 + 1 Calculation (Gray Triangles) and Computed Runup Values Using a Hybrid 2 + 1 and 1 + 1 Model (Empty Circles)

nami was anticipated to be fairly long. Therefore, a threshold computation was at least sensible to first order.

The mechanism of the earthquake source was complex and still is not fully understood. It appears that this was not a typical interplate subduction earthquake, but instead, the plate buckled perpendicular to the subduction line. The Harvard CMT determination was obtained almost 6 h after the main shock and suggested a double-couple solution consisting of two planes, none of which can be considered to represent the low-angle thrust typical for the subduction region interplate event. The model source parameters were $L \times W = 120 \times 100$ km, strike angle = 152°, dip angle = 51°, slip angle, 11°, and $u_0 = 10$ m. The moment magnitude was $M_0 = 3.6 \times 10^{21}$ N/m, assuming $\mu_e = 3 \times 10^{11}$ N/m^2. Using these parameters and the elastic model, the seafloor displacement was calculated (Fig. 5).

The results of the 5-m threshold computation are compared with the measurements on Fig. 5. Note that it has been standard practice among the tsunami hydrodynamics community to use the wave height at the 10-m contour to infer the runup. Reasons for this have been that (1) before 1993 no 2 + 1 inundation computations were possible (Liu et al. 1991; Synolakis 1995), (2) to avoid the unpleasant possibility of wave breaking, and (3) because the lack of topography data would make such computations meaningless. Whether the inference of the runup from the wave height predictions at some threshold level is any less meaningless remains to be proven and is further discussed in the following paragraph.

Fig. 5 shows that the 5-m threshold model reproduced to first order the pattern of the runup distribution along the coasts close to the tsunami source, even without inundation computations. Given the qualitative agreement between the field runup data and the predictions, it is clear that the wave height did not change significantly from the 5-m depth to its maximum runup, suggestive of slow flooding as was also inferred from the survey observations.

The 2 + 1/1 + 1 Hybrid Computation Applied to 1996 Peru Tsunami

On February 21, 1996 at 12:51 GMT (7:51 local time), an $M_w = 7.5$ large earthquake occurred at 9.6°S, 80.2°W, approximately 240 km off the coast of Peru. The available data suggest a low-angle thrust subduction of the Nazca plate beneath the South American plate with complex and relative slow rupture characteristics. The tsunami resulting from this quake impacted more than 300 km of the Peruvian coast causing 12 fatalities, numerous injuries, and property damage.

The ITST surveyed the areas of the tsunami devastation along the Peruvian coast 1 month after the event, between March 15 and 22, 1996 (Bourgeois et al. 1997). The coast of Peru in the affected area is arid with large areas of wind-blown sand. The beaches are wide and fairly plane with very flat slopes, or sheltered curved beaches anchored by rocky outcrops, with somewhat steeper slopes. There is very little vegetation outside of irrigated areas. Thus traditional evidence of tsunami attack, such as dead vegetation, were often absent. Runup heights primarily were based on the debris lines, which in this region can be erased easily by the blowing sand. Runup heights generally varied between 2 and 3 m, except in areas where tsunami focusing occurred. At the Port of Chimbote the tsunami inundated landward 800 m of a 3-m-high, 1-km-long dock, overturning a truck and transporting a steel guard shack over 20 m onshore.

Although the runup heights were not extremely high, inundation distances were often quite large because of the flat beach slopes. At Ensenada La Posa, the tsunami inundated an entire isthmus, approaching from both sides to a distance of 1,500 m and carrying fishing boats 300 m inland. Eyewitnesses generally reported mild or no shaking, and in some areas an LDN wave, causing the shoreline to retreat initially before advancing. The ITST measured topographic transects in four locales.

This event was modeled using the 5-min digital bathymetry (TOPO-5) available from National Oceanic and Atmospheric Administration through the Internet. The nearshore area was corrected using nautical charts down to a resolution of 600 m in many nearshore areas. Even with this resolution, small-scale offshore or onshore features were lost between grid points, rendering any inundation computations meaningless. Instead, a reflective wall was used at the initial shoreline to perform a 2 + 1 computation everywhere, except where the ITST measured transects, where a 1 + 1 inundation computation was used. Again, any justification for such a hybrid computation is really subjective and its usefulness remains to be proven.

The source parameters were derived from the Harvard CMT, as $L \times W = 120 \times 60$ km, strike angle = 340°, dip angle = 15°, slip angle = 96°, and $u_0 = 4$ m. The moment magnitude was $M_0 = 5.6 \times 10^{20}$ N/m, with $\mu_e = 2 \times 10^{11}$ N/m^2. Using these parameters and the elastic model, the seafloor displacement was calculated (Fig. 6). The source produced an LDN propagating toward the shoreline in the area between Huanchaco and Huarmey, consistent with the eyewitness reports, and an LEN elsewhere.

Fig. 6 shows a comparison of the computed tsunami heights using both the 2 + 1 threshold model and the predictions from the hybrid model where the transect data is available.

There are two locations where the discrepancies between the model and measurements are especially large. On the south, the runup at Culebras was measured as high as 5 m. Only one runup measurement [rated B in the scale of Synolakis et al. (1995)] was found at that high altitude, therefore it might have been very localized splash, not expected to have been reproduced by a 600-m resolution grid. On the north, the area near Trujillo shows a distinct local maximum in the runup distribution. The model suggests wave focusing in this area and computes a local maximum in the distribution of runup heights. However, the difference with measurements is larger here than in other locations. Computations with several different source locations and sizes did not significantly change the computed maximum, suggesting that perhaps localized wave refraction, driven by the local bathymetry at a sub-600-

J. Waterway, Port, Coastal, Ocean Eng. 1998.124:157-171.

m scale, influenced the runup. Another explanation would be a more complicated source mechanism with several subfaults. Without studies using higher-resolution topographic and bathymetric data, it is not possible to resolve this discrepancy.

Fig. 6 also shows the results of the hybrid runup computations. The runup modeling was performed at four locations where the ITST measured beach profiles. The input to the 1 + 1 computation was the wave profile computed by the 2 + 1 computation at the 100-m contour, chosen because the 2 + 1 computations showed that the wave was essentially a plane wave beyond this depth. The runup modeling was performed on a 20-m grid. The vertical runup computed by the hybrid model did not differ substantially from the 2 + 1 computations, perhaps a reflection of the slow drop and rise of the water surface. However, the hybrid computations allowed determination of the time evolution of overland flooding. Fig. 7 shows the snapshots of the wave evolution at two different locales, at Rio Santa and at Campo Santa.

At Campo Santa, the runup height was inferred from the debris line, which stretched along the shoreline 455 m inland at an elevation of 1.21 m, both corrected for tidal fluctuations. The topography there consisted of a lagoon extending along the shoreline with a bottom level lower than the mean sea level along the coast. The computed value of the runup as shown in Fig. 7(a) was 1.9 m, with a 500-m onshore penetration. Interestingly, in the computations after the first and second waves withdrew from the lagoon, the water stayed on the level of the debris line forming a pool of water higher than the mean sea level. This result suggests that the debris line might have been formed by the filling of the lagoon and not by the tsunami attack, consistent with what an eyewitness reported.

The computed 3.4-m runup and 390-m penetration distance in Rio Santa compare adequately with the 3.2 and 390-m measurements. The calculation shown in Fig. 7(b) showed that the first wave climbed over the beach step and penetrated inland but that the second wave did not overtop the beach step.

The 2 + 1 Propagation and Inundation Computation for 1993 Okushiri Tsunami

The M_w = 7.8 Hokkaido-Nansei-Oki earthquake of July 12, 1993 was perhaps the most interesting of the recent tidal wave catastrophes. Both high-quality runup data were measured, and fairly unambiguous ground deformation contours were determined due to the proximity to seismic instrument arrays. Most of the damage was concentrated around Okushiri Island off Hokkaido, where extreme runup heights ranging up to 30 m were measured and inundation velocities up to 20 m/s were inferred from structural damage. At the same time, high-resolution bathymetry data are available. It is therefore an ideal test case for evaluating the predictive capabilities of model for extreme events.

Hydrodynamic computations reported to date (Myers and Baptista 1995; Satake and Tanioka 1995; Takahashi et al. 1995) using the SW approximation demonstrated that the hydrodynamic models are able to reproduce to first order the general patterns of the runup height distribution along the coast of Hokkaido and, to some extent, around Okushiri. Unfortunately, they were unable to reproduce wave current velocities and the extreme runup values observed in the front of the island. Even the best available predictions of Takahashi et al. (1995) have differed by a factor of two from the field data for the extreme runup heights.

This simulation will use the three-fault plane dipole-shaped ground deformation model referred to as DCRC-17 of Takahashi et al. (1995) as the initial condition (Fig. 8). DCRC-17 predicts a maximum uplift of 4.2 m and subsidence of 1.1 m. It has produced the closest qualitative agreement with field observations to date among different proposed source models

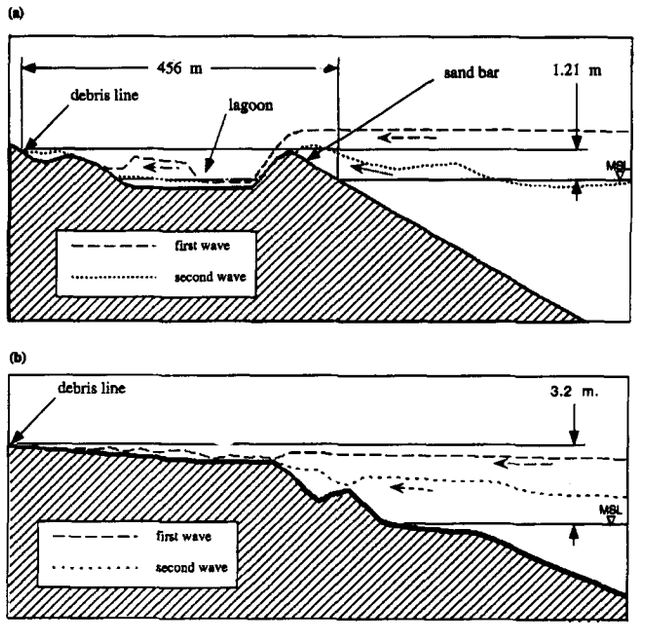

FIG. 7. Surface Profiles Computed with 1 + 1 Runup Model of Tsunami Inundation in: (a) Campo Santa; (b) Rio Santa

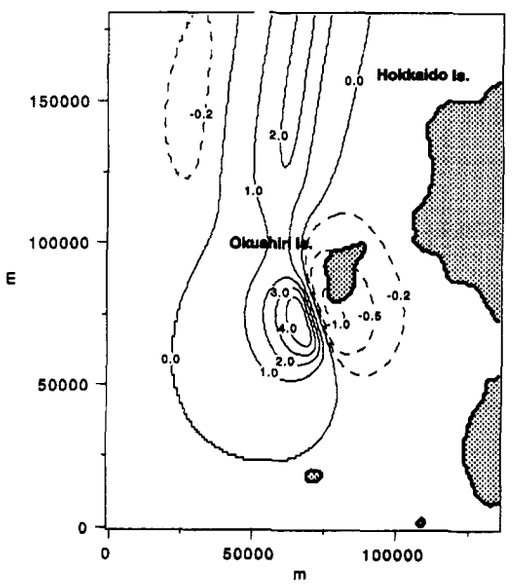

FIG. 8. Contours of Seafloor Displacement of Source Model DCRC-17 of Hokkaido-Nansei-Oki Earthquake Used for Initializing VTCS-3 Computations

(Myers and Baptista 1995; Satake and Tanioka 1995; Takahashi et al. 1995).

The digitized bathymetry for the numerical experiments was generously provided by the Disaster Control Research Center in Tohoku University. It consists of several nested bathymetric arrays with three levels of grid resolution. The main array contains the entire area of computation with a grid size of 450 m^2, and covers a large area of the Sea of Japan, including the source area, Okushiri Island and West coast of Hokkaido Island. The area around Okushiri Island was covered by several nested arrays with a 150-m^2 grid. Near Aonae and Monai, where 50 m^2 data is available, computations using all three available resolutions of the bathymetry were performed, to investigate the influence of the spatial grid size on the results.

Fig. 9 shows the distribution of computed runup heights around Okushiri using VTCS-3 and compares them with the field measurements (Hokkaido Tsunami Survey Group 1993;

J. Waterway, Port, Coastal, Ocean Eng. 1998.124:157-171.

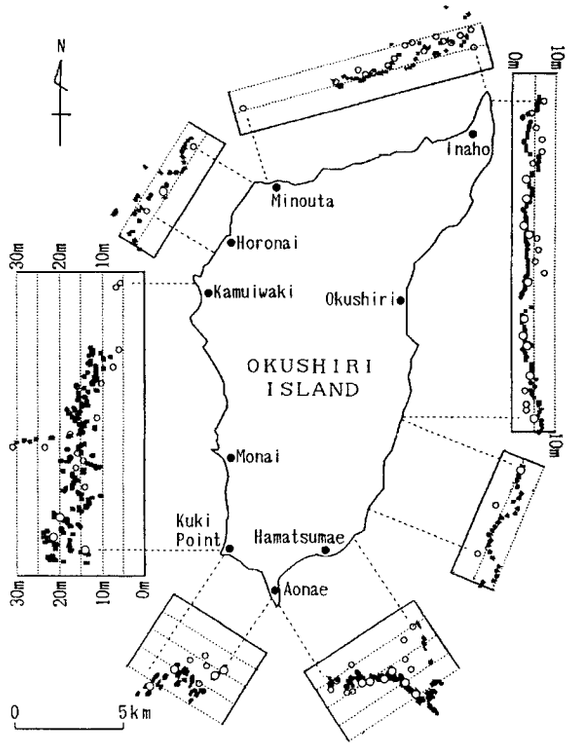

FIG. 9. Comparison of Computed Runup Heights with Field Measurements for Hokkaido-Nansei-Oki Tsunami

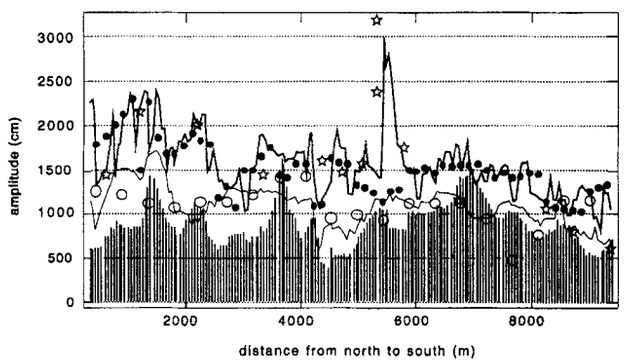

FIG. 10. Comparison of Computed Runup Heights among Computations Using Different Grid Resolutions and Different Types of Computation Thresholds [The Heavy Line, Solid Circles, and Empty Circles are Model Predictions Including Inundation Computations Using a 50, 150, and 450-m Grid, Respectively. Vertical Bars Are Inferred Runup Heights Using a 10-m Depth Threshold in the 50-m Grid Calculation, i.e., Wave Height at 10-m Depth if Vertical Wall Was There. The Thin Line is the Maximum Wave Height at the 10-m Depth Contour for the 50-m Grid Inundation Computations. Stars are the Runup Measurements (Shuto and Matsutomi 1995)]

Shuto and Matsutomi 1995). The computed distribution of the maximum runup heights reproduces most features of the field measurements very well. The extreme 31.7-m measurement near Monai was computed as 29.7 m. The measurement was made at the tip of a small canyon and is undoubtedly a local effect even though all measurements around it were consistently high with a global maximum at 31.7 m, similar to the distribution of computed values shown in the figure. This suggests that the high runup may not have resulted just from the local inland topography, but also from the numerous small-scale features of the nearshore bathymetry. Most computed runup values are slightly higher than measured, but then this model does not include any dissipation. The largest difference is near Inaho in the north, where the calculations predict 15-m heights compared with the 10-m field measurements. Interestingly, 12–15 m field measurements have been reported at Inaho by other Japanese reconnaissance teams. (Nakasuji and Takahashi 1993). Overall the SW model appears adequate for modeling runup heights, suggesting that wave breaking and bottom friction are apparently not important to first order for predicting inundation, at least for this extreme event.

Fig. 10 presents results from numerical experiments which compare the predictions of models with 10-m contour calculation thresholds. These models are still ubiquitous (Imamura et al. 1993; Satake et al. 1993; Yeh et al. 1993; Synolakis et al. 1995; Satake and Tanioka 1995). They propagate the wave using an NSW model up to the 10-m contour, and then use the maximum wave height at that location to infer the maximum runup height. For identical grid resolutions, the results show that interrupting the computation at the 10-m depth, a step essentially equivalent to placing reflective "wall"-type boundaries at that depth, underpredicts the runup by a factor of two, as compared with the inundation computations. Even the computed maxima at the 10-m contour from the full inundation calculation differ substantially from the computed maxima from the 10-m threshold wall calculations, suggesting that the practice of using the wave height at the 10-m depth to infer the runup to first order needs to be reevaluated. Clearly, the wave evolves substantially as it propagates from the 10-m depth up the beach to its maximum runup.

A challenging computation for the SW theory is overland flow. This is a condition where waves overtop a peninsula or a narrow strip of land sandwiched between the ocean and a tidal inlet and then propagate over it and then drain on the lee side of the land. Overland flow has been identified by Synolakis et al. (1995) as one of the leading causes of the heavy casualties during tsunami attack because of the high flow velocities. Note that during tidal wave runup on a sloping beach, the shoreline front slows down as its kinetic energy is converted into potential energy. However, during overland flow over flat land the kinetic energy is reduced only by dissipation. Overland flow is usually supercritical with bore-like dynamics.

Fig. 11 presents overland flow results near Aonae in the four flow snapshots, before, during, and after the overland flow. The last snapshot in Fig. 11(d) shows the inundation of the shore on the east from Aonae Cape. The dynamics are very similar to those inferred from the field observations (Shimamato et al. 1995). The model visualization reveals another in-

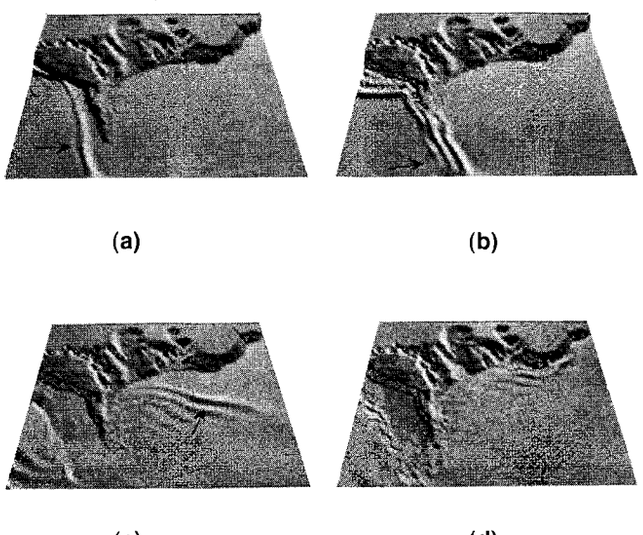

FIG. 11. Bird-Eye Views of Computed Tsunami Wave Overflowing Aonae Cape (Arrows Show Wavefront Propagation Direction)

J. Waterway, Port, Coastal, Ocean Eng. 1998.124:157-171.

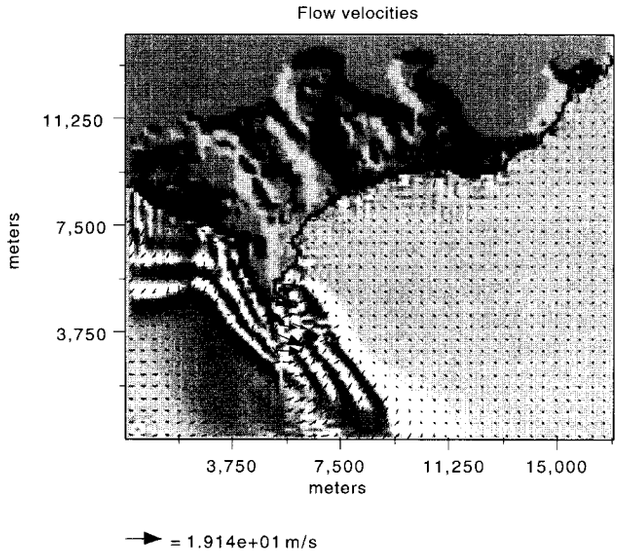

FIG. 12. Flow Velocities Distribution During Overland Flow in Aonae 375 s after the Tsunami Generation (Instantaneous Inundation Boundary Is Also Shown)

teresting phenomenon of the inundation dynamics, the formation of a hydraulic shock or standing bore, during rundown. The hydraulic shock was formed on the west side of the Aonae Cape when the water was receding after the first wave. The shock line formed along the west shore is seen on Fig. 11(c and d). In this location, the waterline recessed down to the 10-m depth, which is approximately 500 m from the original shoreline [Fig. 11(d)]. No eyewitness confirmation of this result was found published anywhere, possibly because the tsunami occurred during nighttime. Numerous eyewitness accounts of such distant water withdrawal during several other tsunami events indirectly support the computed estimates. The snapshot of flow velocities shown in Fig. 12 suggests values in the range of 10–19 m/s over the Aonae peninsula, consistent with the 10–18 m/s field estimates in Aonae (Shimamato et al. 1995).

Fig. 13 presents the envelope of maximum tsunami heights and maximum wave velocities over one typical topographic cross section of Aonae Cape. Notice that the highest inundation velocities occur at the east side of Aonae where inundation heights are smallest. The extreme velocities correlate well with the most devastated area. This is entirely consistent with the fact that during the lee-side rundown of the overland flow, the flow depths are small, but the flow is supercritical with large flow velocities. This underlines the risk of relying exclusively on runup heights to predict inundation.

To further illustrate the significance of the flow velocities for the estimation of the tsunami inundation, the distribution of the maximum velocities around Aonae were computed. Fig. 14 shows contours of the maximum computed horizontal velocities along with the maximum computed inundation line. It was found that the 5-m/s maximum velocity correlates with zones of violent destruction during the tsunami inundation. Note the low-velocity (less than 5 m/s) area on the right (east) shore of Aonae Cape. This location was protected by higher elevation ground from the first wave that came from the west and caused overflow on the southern part of the cape. The area was flooded by the second wave that came from the east. The aerial photographs indicate that flooded houses in this location did not suffer substantial damage, although right next to these houses on the south is the area of a complete devastation where the overflow with high velocities swept away all structures. The 15-m/s velocity contour indicates the area of extremely high velocities occurred during the overland flow on the east shore of Aonae Cape. The other location of over 15-m/s velocities along the west coast of the Aonae Cape also exhibits high velocities during the water withdrawal. The maximum rundown velocities were computed near the line of the farthest water recession after the first wave.

SUMMARY AND CONCLUSIONS

A numerical model was presented to solve the 2 + 1 NSW over arbitrary topography, without friction factors or artificial viscosity. The model uses a splitting technique allowing the implementation of complicated boundary conditions with variable space steps in each direction and nested fine-resolution grids to resolve the changing scales during wave evolution.

It was found that the model is able to reproduce main features of the wave runup process including overland flow for a wide range of initial wave conditions both for laboratory-scale and geophysical-scale waves. Three different implementations of the method have been presented. When no topographic data are available, only threshold computations were performed stopping the calculation at the 5-m depth contour. The wave height estimates at that location were used to infer the runup, as has been the standard practice in tsunami hydrodynamics for the past 10 years. The second method, a hybrid 2 + 1/1 + 1 computation, was used when the coastal bathymetry showed little longshore variation and the incoming tidal wave has a crest that is parallel to the shoreline far offshore and when topographic transect data are available at selected locations. Finally, when both bathymetric and topographic data are available, inundation computations to the maximum penetration point were performed.

It was found that the accuracy and realism of the solution depends more on the bathymetric and topographic resolution rather than on the numerical grid resolution; interpolating in a coarse grid may improve numerical accuracy but not physical realism. Overall, it was found that a nearshore and onland grid of 150 m is necessary to reproduce the overall runup effects, but that a 50-m grid is needed to reproduce extreme inundation heights. Unexpectedly large inundation velocities have been found, and at least in the case with extreme runup heights, the most severe inundation correlated more strongly with the highest velocity contours than with the maximum runup contour.

The study suggests that numerical solutions of the shallow-water wave equations are a very powerful tool for studying tidal wave runup and there is little doubt that the inundation

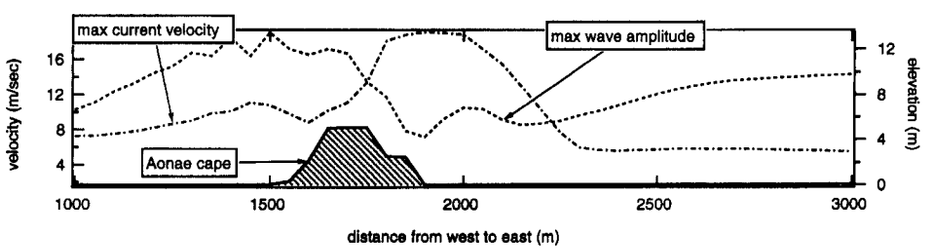

FIG. 13. Computed Envelope of Maximum Tsunami Heights and Maximum Wave Velocities over One Topographic Cross Section of Aonae Cape

J. Waterway, Port, Coastal, Ocean Eng. 1998.124:157-171.

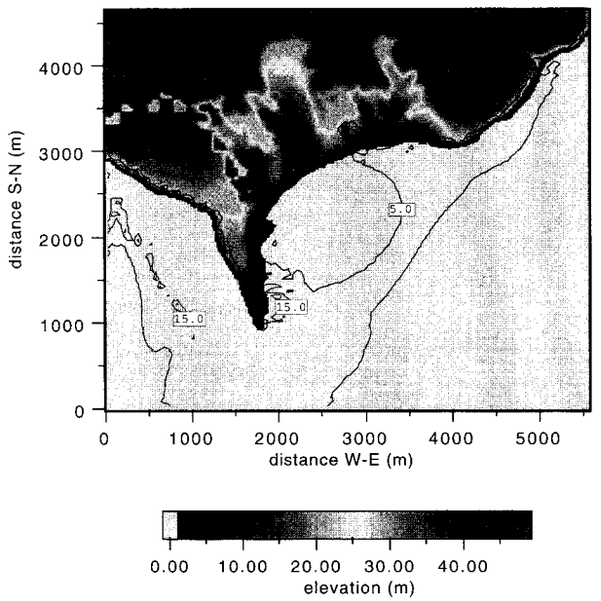

FIG. 14. Contours of Computed Maximum Flow Velocities in Meters per Second over Aonae Cape Area (Computed Maximum Inundation Line Is Also Shown Overlain on Topographic Map)

problem is now solvable. However, unresolved questions remain, in increasing order of importance, as to the effects of friction, the effects of wave breaking, the effects of wave forces on structures in the inundation zone, the time evolution of ground deformation, and the performance of the seafloor displacement models.

ACKNOWLEDGMENTS

The writers thank Dr. Takahashi and Professor Imamura for the digitized bathymetry for the Okushiri tsunami simulation. The writers are grateful to Dr. Cliff Astill of Natural Hazard Program of the National Science Foundation for supporting this research. This study was supported in part by the National Oceanic and Atmospheric Administration Coastal Ocean Program, Contribution No. 1951 from the Pacific Marine Environmental Laboratory, and Contribution No. 490 from the Joint Institute for the Study of the Atmosphere and Ocean.

APPENDIX I. REFERENCES

Bourgeois, J., Petroff, C., Titov, V., Yeh, H., Boyd, and Synolakis, C. (1997). "Tsunami on a coastal desert: The Chimbote, Peru tsunami of 21 February 1996." (submitted to *Pure and Appl. Geophys.*).

Briggs, M. J., Synolakis, C. E., Harkins, G. S., and Green, D. R. (1995). "Laboratory experiments of tsunami runup on circular island." *Pure and Appl. Geophys.*, 144(3/4), 569–593.

Brocchini, M., and Peregrine, D. H. (1996). "Integral flow properties of the swash zone and averaging." *J. Fluid Mech.*, Cambridge, U.K., 317, 241–273.

Carrier, G. F., and Greenspan, H. P. (1958). "Water waves of finite amplitude on a sloping beach." *J. Fluid Mech.*, Cambridge, U.K., 24, 641–659.

Fletcher, C. A. J. (1991). *Computational techniques for fluid dynamics 1*, 2nd Ed., Springer-Verlag, New York.

Fujima, K. (1995). "Application of linear theory to the computation of runup of solitary wave on a conical island." *Long wave runup models*, H. Yeh, P. Liu, and C. Synolakis, eds., World Scientific Publishing Co., River Edge, N.J., 221–230.

Fujima, K., and Shuto, N. (1989). "Friction laws for long waves on dry bed." *Proc., IUGG/IOC Int. Tsunami Symp.*, Novosibirsk, U.S.S.R., 115–119.

Godunov, S. K. (1973). *Finite-difference schemes*. Nauka, Moscow.

Grilli, S. T., and Subramanya, R. (1996). "Numerical modeling of wave breaking induced by fixed or moving boundaries." *Computational Mech.*, 17(6), 374–391.

Grilli, S. T., Subramanya, R., Svendsen, I. A., and Veeramony, J. (1994). "Shoaling of solitary waves on plane beaches." *J. Wtrwy., Port, Coast., and Oc. Engrg.*, ASCE, 120(6), 609–628.

Gustafsson, B., and Kreiss, H.-O. (1979). "Boundary conditions for time dependent problems with an artificial boundary." *J. Comp. Phys.*, 30, 333–351.

Gusyakov, V. K. (1972). "Generation of tsunami waves and oceanic Reayleigh waves by a submarine earthquake." *Mathematical problems of geophysics*, VC SOAN, Novosibirsk, U.S.S.R., 3, 250–272 (in Russian).

Hall, J. V., and Watts, J. W. (1953). "Laboratory investigation of the vertical rise of solitary waves on impermeable slopes." *Tech. Memo. No. 33*, Beach Erosion Board, U.S. Army Corps of Engineers.

Hibbert, S., and Peregrine, D. H. (1979). "Surf and runup on a beach: A uniform bore." *J. Fluid Mech.*, Cambridge, U.K., 95, 323–345.

Hokkaido Tsunami Survey Group (1993). "Tsunami devastates Japanese coastal regions, 1993." *EOS Transactions AGU*, 74(37), 417–432.

Imamura, F., Shuto, N., Ide, S., Yoshida, Y., and Abe, K. (1993). "Estimate of the tsunami source of the Nicaragua earthquake from the tsunami data." *Geophys. Res. Lett.*, 20, 1515–1518.

Iwasaki, R., and Mano, A. (1979). "Two-dimensional numerical simulation of tsunami runup in the Eulerian description." *Proc., 26th Conf. Coast. Engr.*, Japan Society of Civil Engineers, Tokyo, Japan, 70–74.

Kanoglu, U., and Synolakis, C. E. (1995). "Analytical solutions of solitary wave runup on the conical island and on Revere Beach." *Long wave runup models*, H. Yeh, P. Liu, and C. Synolakis, eds., World Scientific Publishing Co., River Edge, N.J., 214–220.

Kobayashi, N., Otta, A. K., and Roy, I. (1987). "Wave reflection and runup on rough slopes." *J. Wtrwy., Port, Coast., and Oc. Engrg.*, 113, 282–298.

Kobayashi, N., and Wurjanto, A. (1992). "Irregular wave setup and runup on beaches." *J. Wtrwy., Harb., Port, Coast., and Oc. Engrg.*, 118(4), 368.

Kowalik, Z., and Bang, I. (1987). "Numerical computation of tsunami runup by the upstream derivative method." *Science of Tsunami Hazards*, 5, 77–84.

Liu, P. L.-F., Cho, Y.-S., Briggs, M. J., Kanoglu, U., and Synolakis, C. E. (1995). "Runup of solitary waves on a circular island." *J. Fluid Mech.*, Cambridge, U.K., 302, 259–285.

Liu, P. L.-F., Synolakis C. E., and Yeh, H. H. (1991). "Report on international workshop on long-wave run-up." *J. Fluid Mech.*, Cambridge, U.K., 229, 675–688.

Mansinha, L., and Smilie, D. E. (1971). "The displacement fields of inclined faults." *Bull. Seismological Soc. of Am.*, 61, 1433–1440.

Masamura, K., and Fujima, K. (1995). "Three-dimensional analysis of long wave runup on a conical island by using the MAC method." *Long wave runup models*, H. Yeh, P. Liu, and C. Synolakis, eds., World Scientific Publishing Co., River Edge, N.J., 321–331.

Meyer, R. E. (1986). "On the shore singularity of water wave theory. II. Small waves do not break on gentle beaches." *Phys. Fluids*, 29, 3164–3171.

Myers, E. P., and Baptista, A. M. (1995). "Finite element modeling of the July 12, 1993 Hokkaido-Nansei-Oki tsunami." *Pure and Appl. Geophys.*, 144(3/4), 769–802.

Nakasuji, T., and Takahashi, M. (1993). *Field report of the July 12, 1993 Hokkaido earthquake*, Kokusai Kogyou, Ltd., Tokyo T102, Japan.

Packwood, A. R., and Peregrine, D. H. (1981). "Surf and runup on beaches: Models of viscous effects." *Rep. No. AM-81-07*, School Math., University of Bristol, Bristol, Conn.

Raubenheimer, B., Guza, R. T., and Elgar, S. (1996). "Wave transformation across the inner surf zone." *J. Geophys. Res., Oc.*, 101(11), 25589–25597.

Satake, K., Bourgeois, J., Abe, K., Tsuji, Y., Imamura, F., Io, Y., Kato, H., Noguera, E., and Estrada, F. (1993). "Tsunami field survey of the 1992 Nicaragua earthquake." *EOS Transections, AGU*, 74(13), 145–156.

Satake, K., and Tanioka, Y. (1995). "Tsunami generation of the 1993 Hokkaido-Nansei-Oki earthquake." *Pure and Appl. Geophys.*, 144(3/4), 803–822.

Shimamato, T., Tsutsumi, A., Kawamoto, M., Miyawaki, M., and Sato, H. (1995). "Field survey report on tsunami disaster caused by the 1993 Southwest Hokkaido earthquake." *Pure and Appl. Geophys.*, 144(3/4), 665.

Shuto, N. (1991). "Numerical simulation of tsunamis." *Tsunami hazard*, E. Bernard, ed., Kluwer Academic Publishers, Doldrecht, The Netherlands, 171–191.

Shuto, N., and Matsutomi, H. (1995). "Field survey of the 1993 Hokkaido-Nansei-Oki tsunami." *Pure and Appl. Geophys.*, 144(3/4), 649–664.

Synolakis, C. E. (1987). "The runup of solitary waves." *J. Fluid Mech.*, Cambridge, U.K., 185, 523–545.

Synolakis, C. E. (1989). "Discussion." *J. Wtrwy., Harb., Port, and Coast., Engrg.*, 115(1), 139.

Synolakis, C. E. (1995). "Tsunami prediction." *Science*, 270, 15.
Synolakis, C. E., Imamura, F., Tinti, S., Tsuji, Y., Matsutomi, H., Cooc, B., and Usman, M. (1995). "The East Java tsunami of the July 4, 1994." *EOS Transactions AGU*, 76(26), 257–261–262.
Synolakis, C. E., and Skjelbreia, J. I. (1993). "Evolution of maximum amplitude of solitary wave on plane beaches." *J. Wtrwy., Harb., Port, and Coast. Engrg.*, 119(3), 323–342.
Tadepalli, S., and Synolakis, C. E. (1995). "The run up of N-waves on sloping beaches." *Proc., Roy. Soc. A*, London, U.K., 445, 99–112.
Tadepalli, S., and Synolakis, C. E. (1996). "Model for the leading waves of tsunamis." *Phys. Rev. Letters*, 77(10), 2141–2144.
Takahashi, To., Takahashi, Ta., Shuto, N., Imamura, F., and Ortiz, M. (1995). "Source models for the 1993 Hokkaido-Nansei-Oki earthquake tsunami." *Pure and Appl. Geophys.*, 144(3/4), 747–768.
Titov, V. V. (1989). "Numerical modeling of tsunami propagation by using variable grid." *Proc., IUGG/IOC Int. Tsunami Symp.*, Novosibirsk, U.S.S.R., 46–51.
Titov, V. V. (1997). "Numerical modeling of long wave runup," PhD thesis, University of Southern California, Los Angeles, Calif.
Titov, V. V., and Synolakis, C. E. (1995a). "Modeling of breaking and nonbreaking long wave evolution and runup using VTCS-2." *J. Wtrwy., Port, and Coast., Engrg.*, 121, 308–316.
Titov, V. V., and Synolakis, C. E. (1995b). "Numerical modeling of 3-D long wave runup using VTCS-3." *Long-wave runup models*, H. Yeh, P. Liu, and C. Synolakis, eds., World Scientific Publishing Co., River Edge, N.J., 242–248.
Yanenko, N. N. (1971). *The method of fractional steps*. translated by M. Holt, Springer, New York, Berlin, Heidelberg.
Yeh, H., Imamura, F., Synolakis, C. E., Tsuji, Y., Liu, P. L.-F., and Shi, S. (1993). "The Flores Island tsunamis." *EOS Transactions AGU*, 74(33), 369, 371–373.
Yeh, H. H., Synolakis, C., and Liu, P. (ed.) (1996). *Long-wave runup models*, World Scientific Publishing Co., River Edge, N.J., Singapore, London, Hong Kong.
Yeh, H., Titov, V. V., Gusyiakov, V., Pelinovsky, E., Khramushin, V., and Kaistrenko, V. (1995). "The 1994 Shikotan earthquake tsunami." *Pure and Appl. Geophys.*, 144(3/4), 569–593.
Zelt, J. A. (1991). "The runup of nonbreaking and breaking solitary waves." *Coast. Engrg.*, 15, 205–246.

APPENDIX II. NOTATION

The following symbols are used in this paper:

d = water depth;
d_0 = initial seafloor displacement;
g = acceleration of gravity;
H = maximum wave height;
h = total height of water column measured from bottom;
h' = epicentral depth of earthquake source;
i = index denoting space discretization;
L = length of rupture plane;
M_0 = moment magnitude;
n = number of time iterations;
p, q, v' = Riemann invariants;
t = time;
u_0 = average slip over rupture plane;
u = horizontal component of depth-averaged velocity in x-direction;
v = horizontal component of depth-averaged velocity in y-direction;
W = width of rupture plane;
x = first horizontal coordinate;
y = second horizontal coordinate;
Δt = time increment;
Δx = space increment along x;
Δy = space increment along y;
Δ_t = forward differencing operator in time direction;
Δ_x = forward differencing operator in x-direction;
Δ_{-x} = backward differencing operator in x-direction;
δ = dip angle;
η = water surface displacement;
θ = strike angle;
λ = eigenvalue; and
μ_e = rigidity of earth's crust.

J. Waterway, Port, Coastal, Ocean Eng. 1998.124:157-171.